LETTERS

# Midzone activation of aurora B in anaphase produces an intracellular phosphorylation gradient

Brian G. Fuller[1]*, Michael A. Lampson[2]*, Emily A. Foley[3], Sara Rosasco-Nitcher[1], Kim V. Le[2], Page Tobelmann[1], David L. Brautigan[4], P. Todd Stukenberg[1] & Tarun M. Kapoor[3]

**Proper partitioning of the contents of a cell between two daughters requires integration of spatial and temporal cues. The anaphase array of microtubules that self-organize at the spindle midzone contributes to positioning the cell-division plane midway between the segregating chromosomes[1]. How this signalling occurs over length scales of micrometres, from the midzone to the cell cortex, is not known. Here we examine the anaphase dynamics of protein phosphorylation by aurora B kinase, a key mitotic regulator, using fluorescence resonance energy transfer (FRET)-based sensors in living HeLa cells and immunofluorescence of native aurora B substrates. Quantitative analysis of phosphorylation dynamics, using chromosome- and centromere-targeted sensors, reveals that changes are due primarily to position along the division axis rather than time. These dynamics result in the formation of a spatial phosphorylation gradient early in anaphase that is centred at the spindle midzone. This gradient depends on aurora B targeting to a subpopulation of microtubules that activate it. Aurora kinase activity organizes the targeted microtubules to generate a structure-based feedback loop. We propose that feedback between aurora B kinase activation and midzone microtubules generates a gradient of post-translational marks that provides spatial information for events in anaphase and cytokinesis.**

It is believed that self-organizing systems position the cleavage furrow, because experimental displacement of the anaphase spindle results in repositioning of the cleavage furrow within minutes[2]. Although mitotic chromosomes are thought to generate gradients of RanGTP that self-organize the prometaphase spindle[3], this cannot be the only self-organizing signal in anaphase because cytokinesis can occur in the absence of chromatin[4,5]. Instead, the location of the cleavage furrow is coupled to the position of the spindle midzone where the chromosome passenger complex containing aurora B kinase is localized. How signals are transmitted over length scales of micrometres between midzone microtubules and the cell cortex is unknown.

To examine spatial patterns of aurora B signalling during anaphase, we developed a strategy using FRET-based sensors that report quantitative changes in substrate phosphorylation in living cells. We adapted a sensor design[6] in which changes in intramolecular FRET between cyan and yellow fluorescent proteins (CFP–YFP) depend on changes in phosphorylation of an aurora B substrate peptide that is conserved among members of the kinesin-13 family[7] (Fig. 1a). To mimic localizations of endogenous aurora B substrates[8], sensors were targeted to centromeres (CENP-B fusion), to chromatin (histone H2B fusion) or to cytosol (lacking targeting sequences) (Supplementary Fig. 1a). To examine the sensor response to changes in aurora B activity in living cells, we first imaged mitotic cells before and after kinase inhibition. Second, we imaged cells through anaphase, when endogenous aurora B substrates are dephosphorylated[9]. For each sensor the YFP:CFP emission ratio increased both after inhibitor treatment and in anaphase, consistent with dephosphorylation for this sensor design[6]. The maximal increase in emission ratio after chemical inhibition is similar to the increase during anaphase for each sensor (Supplementary Fig. 1b), indicating that the measured FRET changes correspond to full dephosphorylation of the sensor.

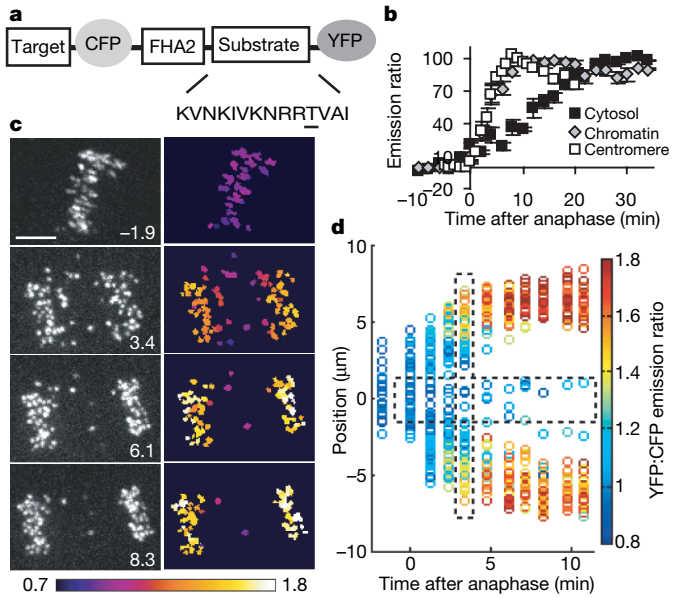


**Figure 1 | A FRET-based sensor of aurora B kinase activity demonstrates a spatial phosphorylation gradient during anaphase.** **a**, Sensor design: phosphorylated threonine is underlined; targeting sequences are from histone H2B (chromatin) or CENP-B (centromere). **b**, HeLa cells expressing cytosolic (untargeted), chromatin-targeted or centromere-targeted sensors were imaged live through anaphase. The YFP:CFP emission ratio at each time point was normalized to vary from 0% to 100% and averaged over multiple cells ($n \geq 4$). Note that increased emission ratio indicates dephosphorylation. **c**, **d**, A HeLa cell expressing the centromere-targeted sensor, with Mad2 depleted by RNAi, was imaged through anaphase. Left panels (**c**), unprocessed YFP images; right panels (**c**), colour-coded images of the emission ratio, timestamps (minutes) relative to anaphase onset. Scale bar, 5 μm. In a plot of all time points (**d**), each circle represents an individual centromere characterized by time after anaphase onset, position along the division axis and emission ratio (colour scale). Dashed lines indicate data points plotted in Supplementary Fig. 4.

[1]Departments of Biochemistry and Molecular Genetics, University of Virginia School of Medicine, Charlottesville, Virginia 22908, USA. [2]Department of Biology, University of Pennsylvania, Philadelphia, Pennsylvania 19104, USA. [3]Laboratory of Chemistry and Cell Biology, The Rockefeller University, New York, New York 10021, USA. [4]Center for Cell Signaling, University of Virginia School of Medicine, Charlottesville, Virginia 22908, USA.
*These authors contributed equally to this work.

To test specificity for aurora B, the cytosolic sensor was treated with a Polo-like kinase (Plk) inhibitor, which did not cause an increase in the emission ratio (Supplementary Fig. 2a). In addition, the cytosolic sensor was not phosphorylated in mitotic cells after aurora B depletion by RNA interference (RNAi) (Supplementary Fig. 2b). Together, these data validate the sensors as reporters of aurora B activity.

To map aurora B kinase activity during anaphase, we examined the kinetics of changes in sensor phosphorylation at different sites. Dephosphorylation of all three aurora B sensors begins immediately after sister chromosome separation and is complete within 8 min for the centromere- and chromatin-targeted sensors, compared with 30 min for the cytosolic sensor (Fig. 1b). This analysis indicates that dephosphorylation kinetics of aurora B substrates in anaphase depend on substrate localization. Mutation of the substrate threonine to alanine, using the chromosomal sensor, eliminated the change in emission ratio (Supplementary Fig. 3).

The rapid dephosphorylation kinetics of the chromosome-targeted sensors are remarkably similar to the kinetics of chromosome segregation, suggesting that phosphorylation changes may be linked to chromosome position during anaphase. To test this possibility, we calculated both the YFP:CFP emission ratio at each centromere (Supplementary Fig. 4a) and its position along the division axis in cells expressing the centromere-targeted sensor. Analysis of single time points early in anaphase, when variance in centromere position is maximal, consistently revealed a correlation between position and sensor phosphorylation (Supplementary Fig. 4b and Supplementary Table 1). These results indicate that although dephosphorylation occurs at all centromeres over time, phosphorylation differences between individual centromeres depend on centromere position.

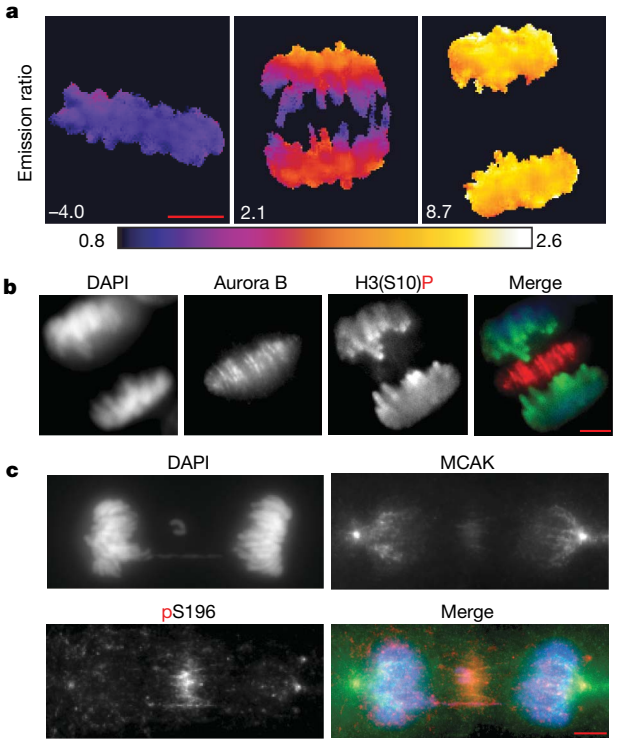


**Figure 2 | The anaphase phosphorylation gradient is observed for multiple aurora B substrates.** **a**, A HeLa cell expressing the chromatin-targeted aurora B sensor was imaged live through anaphase. Colour-coded images of the YFP:CFP emission ratio are shown, timestamp (minutes) relative to anaphase onset. **b**, HeLa cell fixed and stained to label chromosomes (4′,6-diamidino-2-phenylindole (DAPI), blue), H3(S10) phosphorylation (green) and aurora B (red). **c**, *Xenopus* S3 cell fixed and stained for chromosomes (DAPI, blue), MCAK (green) and phospho-MCAK(S196) (red). Scale bars, 5 μm.

To determine the length scale over which position influences sensor phosphorylation, we depleted Mad2 by RNAi to inhibit the spindle checkpoint and increase the variance in centromere positions during anaphase. The sensor is dephosphorylated within 8 min of anaphase onset on centromeres that segregate normally in Mad2-depleted cells, but remains phosphorylated for up to 10 min on centromeres that remain in the centre (Fig. 1c, d and Supplementary Videos 1 and 2). Quantitative analyses demonstrate that changes in sensor phosphorylation depend primarily on centromere position along the division axis, over about 6 μm distance from the centre, rather than on time (Fig. 1d, Supplementary Fig. 4c, d and Supplementary Table 1).

We next examined the chromatin-targeted and cytoplasmic sensors. Spatial phosphorylation patterns were not detected using the cytoplasmic sensor, possibly because rapid diffusion of cytosolic proteins may degrade any spatial patterns so that they are not detected by our methods. The chromatin-targeted sensor revealed a clear phosphorylation gradient. Early in anaphase, sensor phosphorylation is highest on chromatin near the spindle midzone and lowest near the spindle poles (Fig. 2a and Supplementary Videos 3 and 4). Chromosomes segregated normally in these experiments, indicating that microtubule attachments are not perturbed. As the phosphorylation gradient is not restricted to a few individual chromosomes, it is unlikely to reflect differences in chromosome-spindle attachments. A Plk sensor did not reveal spatial phosphorylation patterns in anaphase (Supplementary Fig. 5), which indicates that the phosphorylation gradient is specific for aurora B substrates.

We next examined phosphorylation of endogenous aurora B substrates by immunofluorescence, using phospho-specific antibodies. First we analysed histone H3 serine 10 (H3(S10)) phosphorylation, which was highest in the spindle midzone and lowest towards the poles (Fig. 2b). H3(S10) phosphorylation increased 1.5- to 2.6-fold from pole to midzone in 78% of anaphase cells (60–120 cells per experiment, $n = 6$). This anaphase H3(S10) phosphorylation gradient was verified in multiple cell types and using a second phospho-specific antibody (Supplementary Fig. 6a–d, f). A similar result was reported in *Drosophila* syncitial embryos[10]. Second, we analysed another aurora B substrate, MCAK Ser-196 (ref. 7). During anaphase, MCAK localizes throughout the cell, with highest concentrations at the spindle poles, whereas phospho-MCAK(S196) appears highest in the spindle midzone (Fig. 2c and Supplementary Fig. 6e). Together, these data demonstrate phosphorylation gradients for endogenous and exogenous (FRET sensor) aurora B substrates on chromosomes or the cytoskeleton during anaphase.

To determine whether aurora B localization contributes to formation of the phosphorylation gradient, we used three different perturbations. First, brief (8 min) nocodazole treatment led to microtubule disassembly, spindle midzone disorganization, and dispersion of aurora B throughout the cytoplasm[11] (Fig. 3a and Supplementary Fig. 7b, c). We observed loss of the normal H3(S10) phosphorylation gradient in 76% of nocodazole-treated cells ($n = 110$) (Fig. 3a). Slight increases in H3(S10) phosphorylation were sometimes apparent on chromatin near the spindle midzone, most likely reflecting incomplete microtubule disruption (Supplementary Fig. 7c). Second, we depleted the kinesin MKLP-2 with short hairpin RNAi (shRNAi) (Supplementary Fig. 8b, c), leading to loss of midzone localization of aurora B in 63% of anaphase cells ($n = 27$)[12] and absence of the H3(S10) phosphorylation gradient in 70% of these cells (Fig. 3b). Third, after expression of non-degradable cyclin B, aurora B remained on chromosome arms in anaphase[11,13], and the H3(S10) phosphorylation gradient was disrupted (Supplementary Fig. 7e). Together, these findings indicate that the anaphase phosphorylation gradient depends on aurora B localization to the spindle midzone.

We next addressed how a gradient might be established. One of the best examples occurs during development, when morphogen gradients are produced by self-organizing systems that require localization of an activator and positive feedback[14]. To determine where aurora B

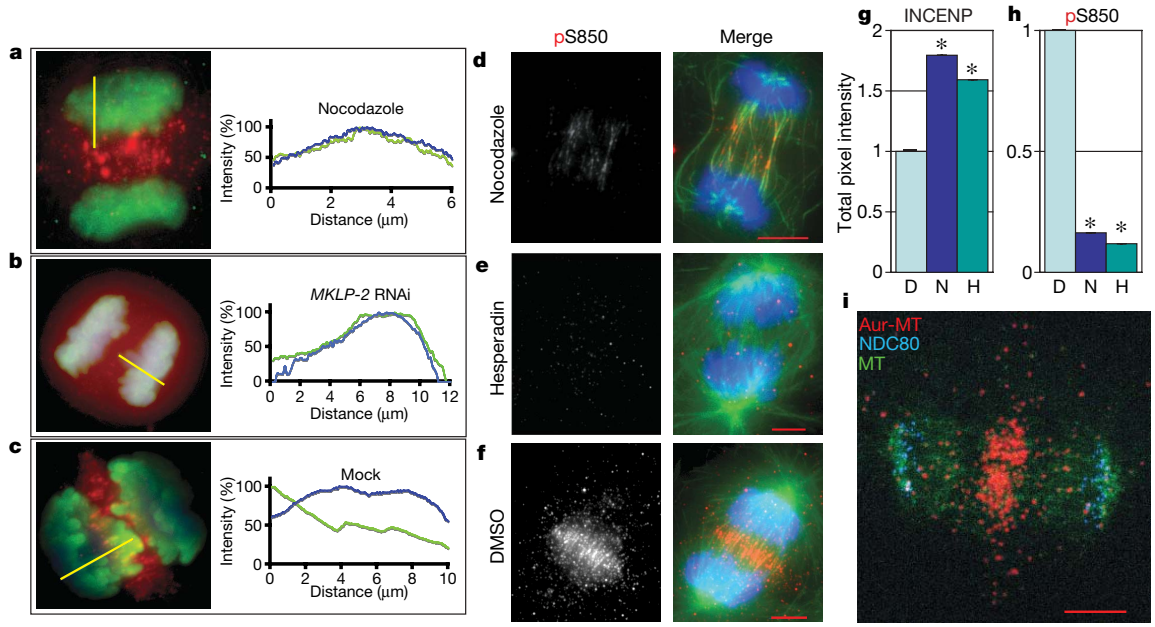


**Figure 3 | The anaphase phosphorylation gradient requires aurora B localization to the midzone, where it is activated.** **a**–**c**, HeLa cells treated with nocodazole for 8 min (**a**), shRNA against *MKLP-2* (**b**) or mock transfected (**c**) were fixed and stained for chromosomes (DAPI, blue), H3(S10) phosphorylation (green) and aurora B (red). Intensity profiles show H3(S10) phosphorylation (green) and DAPI (blue) measured along lines in merged images, with distance increasing away from the midzone. **d**–**f**, *Xenopus* S3 cells treated for 8 min with nocodazole (**d**), hesperadin (**e**) or dimethylsulphoxide (DMSO) (**f**) were fixed and stained for chromosomes (DAPI, blue), tubulin (green) and phospho-INCENP(S850) (red). Total cellular INCENP and phospho-INCENP(S850) in anaphase were measured by quantitative confocal microscopy (**g**–**h**) (mean ± s.e.m., $n \geq 10$, $^*P < 0.005$; D, DMSO; N, nocodazole; H, hesperadin). **i**, Antibodies against tubulin and aurora B were used in a P-LISA in an anaphase *Xenopus* S3 cell; P-LISA product (Aur-MT red), tubulin (MT green), kinetochores (NDC80, light blue). Scale bars, 5 μm.

is activated during anaphase, we analysed phosphorylation of inner centromere protein (INCENP) at serine 850 (INCENP(S850)) in *Xenopus* cells (Supplementary Table 2) and aurora B Thr-232 phosphorylation in HeLa cells. Both modifications are associated with full aurora B activation[15,16]. Using phospho-specific antibodies we found that both INCENP(S850) and aurora B(T232) phosphorylation are limited to the spindle midzone (Fig. 3f and Supplementary Fig. 6f), indicating that aurora B activation is restricted to this site. Brief (8 min) treatment with an aurora B inhibitor, hesperadin[17], led to disruption of midzone microtubule organization (Fig. 3e and Supplementary Fig. 9a, d) and reduction of total phospho-INCENP(S850) staining by 88% (Fig. 3e, h and Supplementary Table 3). Loss of phospho-INCENP(S850) is not caused by a decrease in INCENP protein, as hesperadin treatment increased total INCENP staining during anaphase by over 70% (Fig. 3g and Supplementary Fig. 9a, g). Together, these data suggest that aurora B must be continuously activated during anaphase, and that active kinase localizes to the spindle midzone.

To test the possibility that aurora B activation depends on microtubule association in anaphase, INCENP(S850) phosphorylation was examined after nocodazole treatment, which led to 85% reduction in phospho-INCENP(S850) (Fig. 3d, h). Brief nocodazole treatment did not de-polymerize all microtubules, and residual phospho-INCENP(S850) was confined to the remaining midzone microtubules. Nocodazole treatment also reduced anaphase H3(S10) phosphorylation by approximately 50% (Supplementary Table 4). Microtubules directly stimulated aurora B kinase activity *in vitro* (Supplementary Fig. 10a, b), consistent with previous results[18]. To determine if aurora B directly contacts microtubules during anaphase, we performed a proximity ligation *in situ* assay[19] (P-LISA). The P-LISA product was detected primarily within the spindle midzone, consistent with a direct interaction between midzone microtubules and aurora B (Fig. 3i). This signal co-localized with both markers of aurora B activation, phospho-INCENP(S850) and phospho-aurora B(T232), but not the bulk of tubulin (Supplementary Fig. 10c, d). Together, these data indicate that aurora kinase activity at the spindle midzone is continuously maintained through local interactions with microtubules.

Formation of a phosphorylation gradient centred at the spindle midzone suggests a mechanism to communicate the position of the midzone to the cortex. Although inhibition of aurora B or of midzone components such as MKLP-2 perturbs cytokinesis, it is difficult to separate the function of the gradient from other functions of these proteins. To test whether the gradient may provide spatial information to position the cleavage furrow, we changed the shape of the gradient by perturbing the spatial organization of the anaphase spindle. In the presence of a kinesin-5 inhibitor, spindles are monopolar but anaphase still occurs if the spindle checkpoint is inhibited. Chromosomes are pulled to one side of the cell, followed by microtubule stabilization and cell cleavage on the opposite side[20]. This assay introduces a dramatic spatial change without directly inhibiting aurora B or other midzone or furrow components. We observed a phosphorylation gradient within $1.5 \pm 0.5$ min (mean ± s.e.m., $n = 6$) of chromosome movement in monopolar anaphase. Maximal phosphorylation in the gradient was oriented towards the ingression sites of the cleavage furrow as it forms (Fig. 4a and Supplementary Videos 5–7). Although we did not always observe a cleavage furrow in monopolar anaphase, the gradient was consistently oriented with maximal phosphorylation opposite the direction of chromosome movement (9 out of 12 cells examined) (Supplementary Fig. 11a, b). These results demonstrate that gradient formation is robust to changes in spindle geometry. We also found that aurora B disappears from centromeres in a monopolar anaphase and subsequently redistributes to the cortex where the cleavage furrow forms (Supplementary Fig. 11c, d and Supplementary Videos 8 and 9), beginning $3.1 \pm 0.2$ min (mean ± s.e.m., $n = 5$) after chromosome movement. As the gradient precedes both cortical aurora B localization and furrow ingression, these data suggest that the anaphase phosphorylation gradient provides spatial information to position the cleavage furrow.

Formation of the cleavage furrow depends on signals from the spindle midzone, but how the midzone is initially established is unknown. We propose that release of active aurora B from centromeres establishes a phosphorylation gradient early in anaphase (Fig. 2a), so that substrates known to regulate microtubule organization[1] are preferentially phosphorylated at the centre of the anaphase spindle. The phosphorylation gradient is maintained through a positive feedback loop in which aurora B activity organizes midzone microtubules, and the midzone catalyses local aurora B autophosphorylation of chromosome passenger complex activation sites. Active aurora B diffuses in the cytosol until it is inactivated through dephosphorylation by cytosolic phosphatases (Fig. 4b). Many aurora B substrates are localized to chromosomes or the cytoskeleton, which would limit their diffusion and maintain gradient information. Although we favour this model, we cannot exclude alternatives, for example involving spatial patterns of phosphatase activity.

We have shown that perturbations that block cytokinesis (nocodazole[21], hesperadin[17], *MKLP-2* RNAi[22] and non-degradable cyclinB[13]) also inhibit gradient formation (Supplementary Figs 7i and 8d). Moreover, the relationship between gradient direction and furrow location persists in monopolar anaphase. We propose that the anaphase phosphorylation gradient, which extends over length-scales of micrometres, provides a signalling mechanism to communicate the location and orientation of the spindle midzone to the cell cortex to position the cleavage furrow. Our molecular dissection has uncovered the underlying regulatory basis for an anaphase phosphorylation gradient, and our quantitative analysis of phosphorylation dynamics will lend itself to future mathematical modelling of spatial patterning in anaphase.

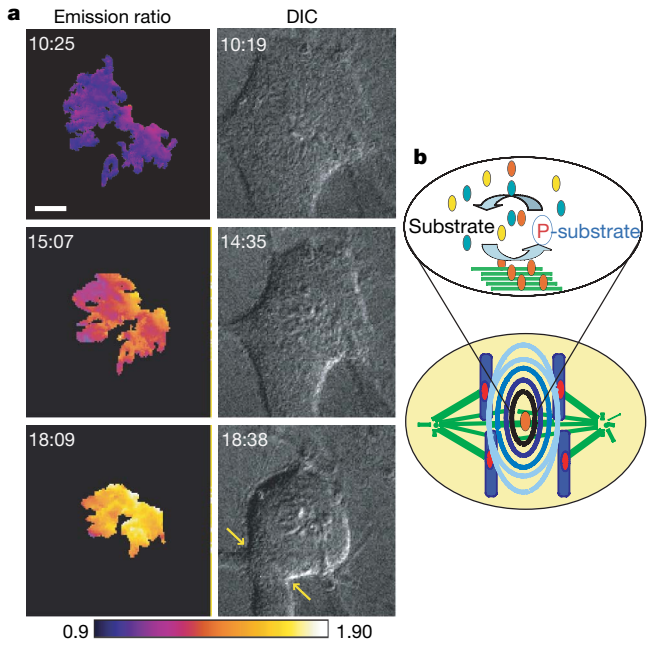


**Figure 4 | The phosphorylation gradient in a monopolar anaphase predicts the cleavage site. a**, A HeLa cell expressing the chromatin-targeted sensor was depleted of Mad2 by RNAi and imaged through anaphase in the presence of the kinesin-5 inhibitor monastrol. Differential interference contrast (DIC) images show chromosome movement and cleavage-furrow formation. Colour-coded images show the YFP:CFP emission ratio, with higher phosphorylation (lower ratio) oriented towards the sites of furrow ingression (arrows). Timestamps minutes:seconds; scale bar, 5 μm. **b**, Model showing that after activation on midzone microtubules, aurora B remains active until dephosphorylation by cytosolic phosphatases. The resulting phosphorylation gradient (contour lines) extends from the midzone to the cortex (yellow ovals, aurora B complex; orange ovals, active aurora B complex; teal ovals, phosphatase).

## METHODS SUMMARY

The aurora B phosphorylation sensor is designed so that the efficiency of intramolecular energy transfer between CFP and YFP depends on the phosphorylation state of the substrate peptide, through reversible binding to an FHA2 phospho-threonine binding domain[6]. The substrate sequence was selected to minimize phosphorylation by other kinases[23] and optimized for binding to the FHA2 domain[24]. Further details of the sensor designs are provided in Methods.

For centromere- and chromatin-targeted sensors, live imaging was performed with a spinning disk confocal microscope (Yokogawa). CFP was excited at 440 nm, and CFP and YFP emissions were acquired simultaneously with a beamsplitter (Dual-View, Optical Insights). Maximal intensity projections are shown for YFP emissions to show sensor localization.

Custom software was written in Matlab (Mathworks) for image analysis. For the centromere-targeted sensor, we designed image-analysis algorithms to identify individual centromeres in three dimensions from confocal image stacks and to calculate the YFP:CFP emission ratio at each centromere. The sensor response at individual centromeres is then described by a multi-dimensional data set consisting of each centromere's spatial coordinates, sensor phosphorylation state as represented by the YFP:CFP emission ratio, and time. The projection of centromere position onto the division axis was calculated to collapse the data set to three dimensions: position as distance from the centre of the separating chromosomes, time after anaphase onset, and emission ratio. Further details of the image analysis are provided in Methods.

For the P-LISA assay, oligonucleotides were directly conjugated to anti-*Xenopus* aurora B and anti-tubulin antibodies. The close proximity of these two antibodies was detected by adding two additional oligonucleotides that could form a template for rolling-circle replication after ligation. The rolling-circle product was then detected by hybridization of fluorescent probes.

**Full Methods** and any associated references are available in the online version of the paper at www.nature.com/nature.

**Received 11 December 2007; accepted 12 March 2008.**
**Published online 7 May 2008.**

1. Glotzer, M. The molecular requirements for cytokinesis. *Science* **307,** 1735–1739 (2005).
2. Bement, W. M., Benink, H. A. & von Dassow, G. A microtubule-dependent zone of active RhoA during cleavage plane specification. *J. Cell Biol.* **170,** 91–101 (2005).
3. Kalab P., Pralle A., Isacoff E. Y., Heald R. & Weis K.. Analysis of a RanGTP-regulated gradient in mitotic somatic cells. *Nature* **440,** 697–701 (2006).
4. Rappaport, R. *Cytokinesis in Animal Cells* (Cambridge Univ. Press, Cambridge, 1996).
5. Alsop, G. B. & Zhang, D. Microtubules continuously dictate distribution of actin filaments and positioning of cell cleavage in grasshopper spermatocytes. *J. Cell Sci.* **117,** 1591–1602 (2004).
6. Violin, J. D. *et al.* A genetically encoded fluorescent reporter reveals oscillatory phosphorylation by protein kinase C. *J. Cell Biol.* **161,** 899–909 (2003).
7. Lan, W. *et al.* Aurora B phosphorylates centromeric MCAK and regulates its localization and microtubule depolymerization activity. *Curr. Biol.* **14,** 273–286 (2004).
8. Ruchaud S., Carmena M. & Earnshaw W. C.. Chromosomal passengers: conducting cell division. *Nature Rev. Mol. Cell Biol.* **10,** 798–812 (2007).
9. Zeitlin, S. G. *et al.* Differential regulation of CENP-A and histone H3 phosphorylation in G2/M. *J. Cell Sci.* **114,** 653–661 (2001).
10. Su, T. T., Sprenger, F., DiGregorio, P. J., Campbell, S. D. & O'Farrell, P. H. Exit from mitosis in *Drosophila* syncytial embryos requires proteolysis and cyclin degradation, and is associated with localized dephosphorylation. *Genes Dev.* **21,** 495–503 (1998).
11. Murata-Hori, M., Tatsuka, M. & Wang, Y. L. Probing the dynamics and functions of aurora B kinase in living cells during mitosis and cytokinesis. *Mol. Biol. Cell* **4,** 1099–1108 (2002).
12. Gruneberg, U., Neef, R., Honda, R., Nigg, E. A. & Barr, F. A. Relocation of aurora B from centromeres to the central spindle at the metaphase to anaphase transition requires MKLP2. *J. Cell Biol.* **166,** 167–172 (2004).
13. Wheatley, S. P. *et al.* CDK1 inactivation regulates anaphase spindle dynamics and cytokinesis *in vivo*. *J. Cell Biol.* **138,** 385–393 (1997).
14. Meinhardt, H. & Greier, A. Pattern formation by local self-activation and lateral inhibition. *Bioessays* **22,** 753–760 (2000).
15. Bishop, J. D. & Schumacher, J. M. Phosphorylation of the carboxyl terminus of inner centromere protein (INCENP) by the aurora B kinase stimulates aurora B kinase activity. *J. Biol. Chem.* **277,** 27577–27580 (2002).
16. Yasui, Y. *et al.* Autophosphorylation of a newly identified site of aurora-B is indispensable for cytokinesis. *J. Biol. Chem.* **279,** 12997–13003 (2004).
17. Hauf, S. *et al.* The small molecule hesperadin reveals a role for Aurora B in correcting kinetochore-microtubule attachment and in maintaining the spindle assembly checkpoint. *J. Cell Biol.* **161,** 281–294 (2003).

18. Rosasco-Nitcher, S. E., Lan, W., Khorasanizadeh, S. & Stukenberg, P. T. Centromeric Aurora-B actvation requires TD-60, microtubules and substrate priming phophorylation. *Science* **319,** 469–472 (2008).
19. Söderberg, O. *et al.* Direct observation of individual endogenous protein complexes in situ by proximity ligation. *Nature Methods* **3,** 995–1000 (2006).
20. Canman, J. C. *et al.* Determining the position of the cell division plane. *Nature* **424,** 1074–1078 (2003).
21. Wheatley, S. P. & Wang, Y.-L. Midzone microtubule bundles are continuously required for cytokinesis in cultured epithelial cells. *J. Cell Biol.* **135,** 981–989 (1996).
22. Neef, R. *et al.* Phosphorylation of mitotic kinesin-like protein 2 by polo-like kinase 1 is required for cytokinesis. *J. Cell Biol.* **162,** 863–875 (2003).
23. Obenauer, J. C., Cantley, L. C. & Yaffe, M. B. Scansite 2.0: proteome-wide prediction of cell signaling interactions using short sequence motifs. *Nucleic Acids Res.* **31,** 3635–3641 (2003).
24. Durocher, D. *et al.* The molecular basis of FHA domain:phosphopeptide binding specificity and implications for phospho-dependent signaling mechanisms. *Mol. Cell* **6,** 1169–1182 (2000).

**Supplementary Information** is linked to the online version of the paper at www.nature.com/nature.

**Acknowledgements** We thank: the Department of Biochemistry and Molecular Genetics, University of Virginia School of Medicine, for its support; D. Burke for many discussions; W. Lan for contributions to this manuscript; Y.-L. Wang (University of Massachusetts Medical School) for the aurora B-green fluorescent protein (aurora B-GFP) plasmid; H. Nakagawa (University of Tokyo) for the anti-MKLP-2 antibody; C. D. Allis (Rockefeller University) for the anti-phospho H3 serine 10 antibody; A. Newton (University of California San Diego) for the CKAR plasmid; A. North and the Rockefeller University Bioimaging facility. This work was supported by: the American Lung foundation (P.T.); the National Institutes of Health grants to T.M.K., P.T.S. and D.L.B.; a Francis Goulet Fellowship at Rockefeller University (M.A.L.); a National Institute of Child Health and Human Development T32 Training Grant 'Cellular and Physiologic Mechanisms in Reproduction' at the University of Virginia (B.G.F.); and the Pew Charitable Trust. E.A.F. is a Robert Blount Family Fellow of the Damon Runyon Cancer Research Foundation. We thank N. Kraut and Boehringer Ingelheim for hesparadin.

**Author Contributions** Development of the aurora B and Plk phosphorylation sensors, and FRET imaging and analysis, were done in the Kapoor laboratory by M.A.L. with E. A.F. B.G.F. performed immunofluorescence experiments. S. R.-N. and P.T. performed the kinase assays and P-LISA experiments, respectively. K.V.L. performed live imaging of aurora B-GFP. M.A.L. and B.G.F. wrote the paper.

**Author Information** Reprints and permissions information is available at www.nature.com/reprints. Correspondence and requests for materials should be addressed to P.T.S. (pts7h@virginia.edu) or M.A.L. (lampson@sas.upenn.edu).

## METHODS

**Sensor construction.** The aurora B sensor was generated by modifying the protein kinase C sensor CKAR. The PKC substrate sequence was replaced with KVNKIVKNRRTVAI. This sequence is from HsKif2, residues 57–70, with an Ile inserted at position +3 relative to the Thr to promote binding to the FHA2 domain[24]. Analysis of this sequence with Scansite[23] does not predict phosphorylation of this sequence by any other kinases, even at low stringency. The CyPet–YPet variants of CFP–YFP, which were optimized for FRET[25], were used to maximize sensitivity and the dynamic range of the sensor. Truncation of the substrate sequence or further optimization for FHA2 binding did not improve the sensor response (data not shown).

For targeting to centromeres, residues 1–167 from human CENP-B[26] (Invitrogen, clone ID 6470289) were amplified by PCR and fused to the amino terminus of the sensor. For targeting to chromatin, human histone H2B was amplified from pBOS-H2BGFP (BD Pharmingen) and inserted in place of CENP-B. These sequences have been previously shown to target GFP to the centromere or to chromatin. The Plk sensor was constructed by replacing the substrate sequence in the aurora sensor with LLLDSTLSINWD. This sequence is from Myt1, residues 421–432. The Plk substrate, Ser 426, is replaced with Thr, and an Ile is inserted at 429 to promote FHA2 binding.

**Cell culture, transfection and live imaging.** *Xenopus* S3 cells were maintained in 66% L-15 medium containing 10% FBS, 50 IU $ml^{-1}$ penicillin, 50 mg $ml^{-1}$ streptomycin and 1 mM sodium pyruvate at room temperature. HeLa, Du145 and DLD21 cells were cultured in growth medium, DMEM (Invitrogen) with 10% FBS (Sigma) and penicillin–streptomcyin (100 U $ml^{-1}$ and 100 μg $ml^{-1}$, respectively, Invitrogen), at 37 °C in a humidified atmosphere with 5% $CO_2$.

For live-cell studies, cells were transfected with plasmid DNA using Fugene (Roche Diagnostics) followed in some cases by a second transfection with an siRNA duplex targeting *Mad2* (5′-AAGAGUCGGGACCACAGUUUA-3′, Dharmacon) using Oligofectamine (Invitrogen). Transfection of plasmid DNA and siRNA targeting aurora B (5′-AACGCGGCACUUCACAAUUGA-3′, Dharmacon) were performed simultaneously using Lipofectamine 2000 (Invitrogen) to increase the probability of co-transfection. Aurora B knockdown was verified by immunostaining using a monoclonal antibody (BD Transduction Laboratories) to show that cells expressing the sensor were also depleted of aurora B.

One day after transfection, cells were plated on 22 mm × 22 mm No. 1.5 glass coverslips (Fisher Scientific) coated with Poly-D-lysine (Sigma) and used for imaging the following day. Coverslips were mounted in Rose chambers for live imaging, using L-15 medium without phenol-red (Invitrogen). Temperature was maintained at 35–37 °C, using either a temperature-controlled chamber (Solent Scientific) or an air-stream incubator (ASI 400, Nevtek). The kinesin-5 inhibitor monastrol was used at 100 μM to induce monopolar spindles.

For Plk and aurora B inhibition experiments, cells were first incubated with 0.5 μg $ml^{-1}$ nocodazole (Sigma) to prevent mitotic exit. Cells were imaged live before and after addition of the aurora B inhibitor hesperadin[17] (50 nM) or the Plk inhibitor BTO-1 (20 μM)[27]. The YFP:CFP emission ratio was calculated from images acquired at each time point. Cells were followed until the maximal increase in emission ratio was achieved.

For live imaging of sensors without targeting domains, images were acquired on a Carl Zeiss Axiovert 200M microscope with a 63× 1.4 NA objective, a cooled, back-thinned electron multiplier charge-coupled device camera (Cascade II 512B, Photometrics) and Metamorph software (Universal Imaging). CFP and YFP emissions were acquired sequentially with CFP excitation. CFP and YFP emissions were summed over an entire cell after background subtraction, and the YFP:CFP emission ratio was calculated.

For centromere- and chromatin-targeted sensors, images were acquired on a Carl Zeiss Axiovert 200M microscope equipped with a *z*-motor, a 100× 1.4 NA objective and a Yokogawa spinning disk confocal QLC100 unit. CFP was excited at 440 nm, and both CFP and YFP emissions were acquired simultaneously using a beamsplitter (Dual-View, Optical Insights), a cooled, back-thinned electron multiplier charge-coupled device camera (Hamamatsu, C9100-12) and Metamorph software (Universal Imaging). The pixel size in this configuration was 0.16 μm. Confocal image stacks were acquired with 0.5 μm spacing, typically 12 sections per stack.

**Image analysis of targeted FRET sensors.** Custom software was written in Matlab (Mathworks) for image analysis. CFP and YFP emissions were aligned by minimizing the correlation coefficient between the two images. Background intensities were calculated either locally around each centromere (for the centromere-targeted sensor) or globally around the entire spindle (for the chromatin-targeted sensor). For the chromatin-targeted sensor, intensity thresholds were selected manually, and mean CFP and YFP intensities were calculated over a 5 pixel × 5 pixel square centred on each pixel within the thresholded area. The YFP:CFP emission ratio was calculated from these local means and used to create a ratio image, whereas pixels outside the thresholded area were set to zero. Projections of the ratio images were calculated as the average over the *z*-dimension of all non-zero pixels at each (*x*, *y*) coordinate. The projections were colour-coded for graphical representation of the sensor phosphorylation state at each pixel. The colour scale was set to incorporate the entire range of the emission ratio during anaphase. To plot the change in emission ratio versus position, pixels were binned by distance from the centre of the separating chromosomes, in increments of 1.6 μm, and the average emission ratio calculated for each bin.

For the centromere-targeted sensor, three-dimensional (*x*, *y*, *z*) images were created from the confocal image stacks. The images were made binary using CFP and YFP intensity thresholds. Objects were defined from the binary images as connected pixels in three dimensions with a minimum size of 10 or 20 pixels. The CFP and YFP intensity thresholds used to create the binary images were initially selected manually, and all objects below 100 pixels in size were considered individual centromeres. For objects larger than 100 pixels, the intensity thresholds were locally increased incrementally until all objects were below a maximum size of 100 pixels. This algorithm ensured that centromeres that were close together were not merged into a single large object. Many, but not all, centromeres were separated by this algorithm. Because the intensity threshold was determined locally, both dimmer and brighter centromeres were included in the analysis. For each object, the CFP and YFP intensities were summed, and a single emission ratio was calculated to represent that object in a three-dimensional ratio image. By averaging over multiple pixels, the signal-to-noise ratio was improved dramatically over a pixel-by-pixel analysis. Pixels not included in any object were set to zero. Projections were calculated and colour-coded as described above for the chromatin-targeted sensor.

Preparation of fixed cells, image acquisition and analysis for fixed cells, kinase and proximity ligation assays were performed using standard techniques essentially as described[7,18,19]. These specific techniques are further described in Supplementary Methods.

25. Nguyen, A. W. & Daugherty, P. S. Evolutionary optimization of fluorescent proteins for intracellular FRET. *Nature Biotechnol.* **23**, 355–360 (2005).
26. Shelby, R. D., Hahn, K. M. & Sullivan, K. F. Dynamic elastic behavior of α-satellite DNA domains visualized *in situ* in living human cells. *J. Cell Biol.* **135**, 545–557 (1996).
27. Peters, U. *et al.* Probing cell-division phenotype space and Polo-like kinase function using small molecules. *Nature Chem. Biol.* **2**, 618–626 (2006).